Revealing Main Reaction Paths to Olefins and Aromatics in Methanol-to-Hydrocarbons over H-ZSM-5 by Isotope Labeling

Liu, Chuncheng; Uslamin, Evgeny A.; Pidko, Evgeny A.; Kapteijn, Freek

DOI
10.1021/acscatal.3c00168

Publication date
2023

Document Version
Final published version

Published in
ACS Catalysis

ACS Catalysis

pubs.acs.org/acscatalysis

Research Article

Revealing Main Reaction Paths to Olefins and Aromatics in Methanol-to-Hydrocarbons over H-ZSM-5 by Isotope Labeling

Chuncheng Liu, Evgeny A. Uslamin, Evgeny A. Pidko,* and Freek Kapteijn*

Cite This: *ACS Catal.* 2023, 13, 5205−5212

Read Online

ACCESS | Metrics & More | Article Recommendations | Supporting Information

ABSTRACT: The nature of hydrocarbon pool (HCP) intermediates in the methanol-to-hydrocarbons (MTH) process has been thoroughly investigated, especially for BEA- and CHA-type zeolite catalysts like H-β and H-SAPO-34. Herein, we further reveal the dynamic mechanistic details of the MTH process over the H-ZSM-5 catalyst at 400 °C, based on the dual-cycle mechanism and HCP in this medium-pore zeolite. Application of switching sequences of ^{13}C-labeled and unlabeled methanol pulses over a model H-ZSM-5 catalyst combined with on-line MS analysis and a recently reported technique called "fast scanning-pulse GC analysis" provides a direct and quantitative insight into the MTH reactions under quasi-steady-state conditions. The transient product responses showed the almost instant formation of hydrocarbons upon a small pulse of methanol, followed by secondary formation of light aromatics via HCP decomposition and olefin alkylation−dealkylation, especially in a long catalyst bed when methanol is quickly consumed in the initial reaction zone in the catalyst bed. The isotopic analysis of typical aliphatic C_{3+} product responses after switching ^{13}C-methanol pulses to the unlabeled methanol pulses showed a fast isotope scrambling in the formation of C_{3+} species. MS analysis of the light aromatics indicates a complete consecutive but slower isotope incorporation process of ^{12}C into ^{13}C-aromatics. Results provide direct experimental confirmation of the kinetically preferred olefin-based cycle over the aromatic-based cycle. The sequential isotopic incorporation strongly suggests that the paring reaction pathway through aromatic ring contraction and re-expansion steps is operative. In the appearance of aromatics upon pulsing methanol over larger catalyst beds, four processes are directly discerned, involving the displacement of adsorbed species by formed water, isotope incorporation yielding directly labeled and unlabeled products through the paring mechanism and direct aromatization, and HCP conversion through secondary reactions.

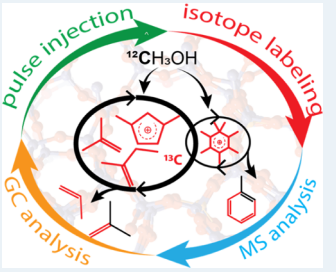

KEYWORDS: *methanol-to-hydrocarbons, $^{13}C/^{12}C$ switch, fast scanning-pulse analysis (FASPA), hydrocarbon pool mechanism, isotope labeling*

INTRODUCTION

The methanol (MeOH) conversion by zeolite catalysts proceeds via a complex network of transformations. This involves cooperation between zeolite Brønsted acid sites and the confined hydrocarbon intermediates, commonly referred to as the hydrocarbon pool (HCP) mechanism.[1−5] Instead of direct conversion, MeOH is first transformed into long linear or cyclic hydrocarbons, which are trapped in the zeolite pores. These bulky intermediates split off light olefins and aromatics like propylene and toluene and may subsequently undergo methylation with MeOH.

Owing to the shape-selectivity feature, distinct HCP species may be generated depending on the zeolite pore size and acid strength, resulting in an entirely different product distribution throughout the MeOH transformation process. Assisted by the fast development of advanced spectroscopy techniques, especially in situ/operando NMR spectroscopy, the identification of these HCP species progresses enormously. For instance, heptamethyl-benzenium ions were detected to be readily formed in H-β, whereas MeOH conversions mainly proceed via penta- and hexa-methylbenzenes in H-SAPO-34 zeolite catalysts. Within the H-ZSM-5 zeolite having a larger channel diameter and possessing channel intersections instead of cavities like H-SAPO-34 has, higher methylbenzenes like penta- and hexa-methylbenzenes are virtually unreactive.[4] Instead, methylated/methylenated five-membered ring cations, as well as tri- and tetramethylbenzenes are proven to be the HCP intermediates.[2,6−13] Meanwhile, the large pore opening (0.5−0.6 nm) of H-ZSM-5 ensures the diffusing out of BTX (benzene, toluene, and xylenes) and trimethylbenzenes (TriMB).

Next to the HCP identity, the kinetic study of MeOH interacting with HCP species leading to final products is rather difficult from a purely experimental point of view due to the complex reaction network and limited spatial-/temporal analysis tools to study the ongoing activities within the zeolite micropore under operational conditions. Particularly, in the H-

Received: January 11, 2023
Revised: March 16, 2023

ZSM-5 zeolite catalyst, the originally formed HCP intermediates rapidly degrade or desorb once the MeOH feeding stops[14] or its conversion is complete,[15] highlighting the dynamic feature of HCP in the medium pore-size H-ZSM-5 zeolite catalysts. So far, transient kinetic techniques, such as the temporal analysis of products (TAP) and $^{12}C/^{13}C$ isotope labeling, have been utilized to obtain highly specific mechanistic and kinetic information about the MTH mechanism.[16,17] However, the challenging transient data analysis relying on mass spectrometry in the TAP setup limits the discrimination of specific individual reaction steps like olefin methylation or cracking in the MTH,[17,18] since they can affect each other in such a complex reaction network. Enormous mechanistic and kinetic information can be extracted from $^{12}C/^{13}C$ labeling experiments. As early as 1982, Dessau and LaPierre used ^{13}C-MeOH cofeeding ^{12}C-olefin/aromatic reactions to study the MTH mechanism. That study reveals that olefins are produced via continuous methylation/cracking, an indirect route.[19] In a later study, Dahl and Kolboe used the isotope labeling technique to further develop this indirect route and proposed the HCP mechanism.[1−5] Furthermore, based on the time evolution of the ^{13}C composition in light olefins and aromatic effluent products after switching from ^{12}C-MeOH feeding to ^{13}C-MeOH feeding in H-ZSM-5, Olsbye and co-workers proposed the dual-cycle mechanism within H-ZSM-5, suggesting that C_{3+} olefins are formed from the methylation and cracking of the longer olefinic intermediates in the so-called olefin cycle, while ethylene and aromatics are formed by methylation and dealkylation of methylbenzenes in the aromatic cycle.[16] Therefore, the isotope labeling technique combined with GC−MS analysis plays a substantial role in the study into the MTH mechanism. However, due to a limited time resolution, the commonly applied off-line GC−MS analysis of collected effluent products and species trapped in the zeolite might miss key information during the fast transient of $^{13}C/^{12}C$-species switching processes. Moreover, the cofeeding of ^{13}C-olefins or aromatics in excess over their real formation levels in the MTH process might saturate the zeolite catalyst, leading to a misunderstanding of the role of these species in the HCP mechanism. Therefore, to achieve this understanding, it is necessary to combine the very high temporal resolution of the method with its chemical specificity and the ability to work under real reaction conditions. Notably, Pérez-Ramírez et al. have recently employed photoion photoelectron coincidence spectroscopy as a new analytical tool that provides extensive information on the reaction intermediates, confirming the key role of dimethylpentenyl species in the MTH mechanism.[20]

We herein present a quantitative analysis of HCP species in H-ZSM-5 zeolite catalysts and their reactivity with MeOH in the MTH process, relying on the isotope labeling technique and the fast scanning-pulse analysis (FASPA[15]). This recently developed FASPA technique allows quantitative GC mapping of the fast temporal evolution of the product responses upon a MeOH pulse over the catalyst. The online MS analysis of different effluent products in the ^{13}C-MeOH/^{12}C-MeOH/water switch pulse experiments directly reveals the highly dynamic character of the HCP in H-ZSM-5 in its contribution to the production of aromatics and light olefins. Four consecutive pathways from MeOH to aromatics are directly and quantitatively discerned under MeOH-pulsing conditions. The $^{13}C-^{12}C$ distribution within various products is assessed semi-quantitatively, showing that light olefins are predominantly produced via the olefin cycle, while light aromatics (and light olefins) are produced via the paring mechanism rather than the side-chain mechanism in the aromatic cycle.

RESULTS

The physicochemical properties of the utilized zeolite catalysts, set-up, and MTH testing conditions can be found in the Supporting Information. To obtain the second resolution in the temporal responses upon MeOH pulse, a synchronizing program in the FASPA approach was used to control the GC sampling with pre-set increasing time delays (from 1 to 225 s before the next MeOH pulse, the time step is 1 s) during the repetitive MeOH pulses (pulse interval of 3.75 and 1.25 min). More technical details and validation of the FASPA approach in the MTH process can be found in Supporting Information and in our previous work.[15] Typical obtained product responses from FASPA tests over H-ZSM-5 are shown in Figure 1.

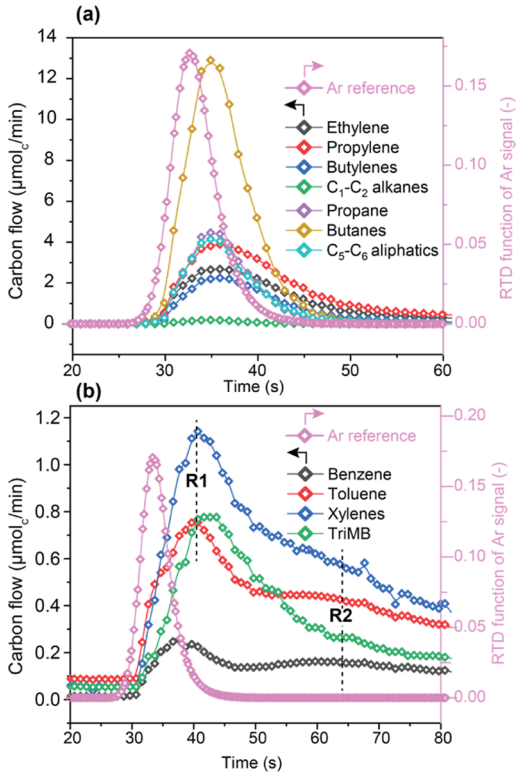

Figure 1. FASPA temporal responses of aliphatic (a) and aromatic products (b) upon MeOH pulsing over the H-ZSM-5 zeolite catalyst. FASPA experimental conditions: T = 400 °C, m_{cat} = 100 mg (H-ZSM-5, Si/Al 25, 150−212 μm), $P_{reactor}$ = 1 bar, MeOH pulse quantity 7.6 μmol_C per pulse, carrier gas He = 20 mL_{NTP}/min, pulse interval = 3.75 min, and time delay = 1 s. Xylenes refer to the sum of *o*-, *m*-, and *p*-xylene. TriMB is the abbreviation of trimethylbenzenes. Ar (MS signal m/z = 40) was used as an inert tracer to account for the set-up response time delay.

Upon a MeOH pulse (7.6 mol_C) to a 100 mg H-ZSM-5 catalyst bed, a clear time delay of ∼1.5 s was observed between the appearance of the co-injected tracer Ar and all formed hydrocarbons, which is attributed to the induction period required to build up or restore the HCP from MeOH until the first hydrocarbon product in the effluent leaving the catalytic bed. From ∼28 s, all aliphatic species (Figure 1a) are observed

https://doi.org/10.1021/acscatal.3c00168
ACS Catal. 2023, 13, 5205−5212

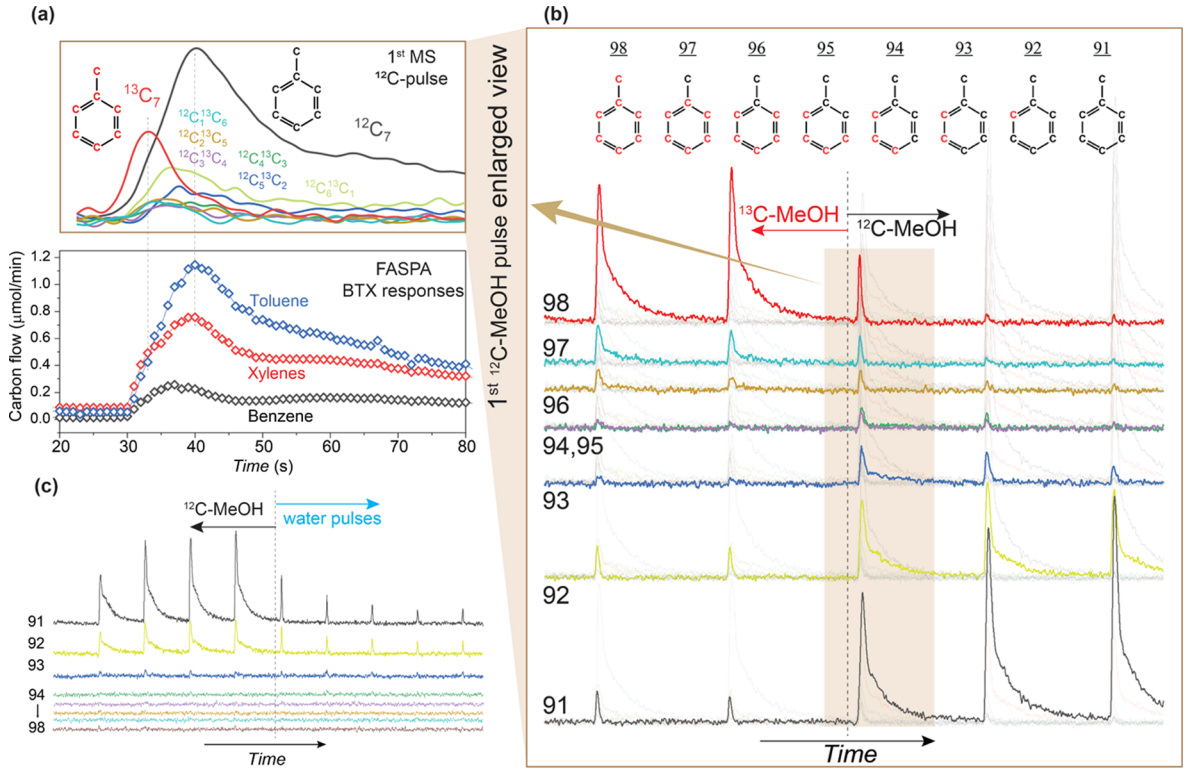

Figure 2. Temporal responses of $^{13}C/^{12}C$-MeOH/H_2O pulse switch experiments. Comparison of BTX (benzene, toluene, and xylenes) responses in the FASPA test and the enlarged view of C_7 isotopic compositions (formula $^{12}C_n{}^{13}C_{7-n}$, n = 0−7) in the first ^{12}C-MeOH pulse after switching from ^{13}C-MeOH (a); full MS fragmentation (m/z = 91−98) responses in the ^{13}C-MeOH ⇒ ^{12}C-MeOH switch test (b); C_7 MS fragmentation (m/z = 91−98) responses in the ^{12}C-MeOH ⇒ H_2O switch test (c). Key: Injection of either ^{12}C− or ^{13}C-MeOH in He, 7.6 μmol_C/pulse or with H_2O-saturated He (~2.4 μmol_{water}/pulse). T = 400 °C, m_{cat} = 100 mg (H-ZSM-5, Si/Al = 25, 150−212 μm), $P_{reactor}$ = 1 bar, carrier gas He = 20 mL_{NTP}/min, pulse interval = 3.75 min. The compositions in (a) were converted from MS fragment responses in (b) (the procedure can be found in Supporting Information).

and rapidly reach their max around ~36 s. After that, these responses slowly decrease to zero in terms of concentration in the exit flow until the end (before the next MeOH pulse). Combined with in situ DRIFT spectroscopy, our previous study revealed that the hydrocarbon productions are closely associated with the HCP build-up within the zeolite upon the MeOH pulse. Once the injected MeOH is rapidly depleted, the decomposition and desorption of the formed HCP species explain the long tailing of observed responses, as shown in Figure 1, demonstrating the dynamic character of the HCP in the medium-pore H-ZSM-5 zeolite catalyst.[15] However, because of measurement limitations, these HCP species cannot be directly identified during FASPA tests. In particular, a sharp first response (R1) is observed for benzene, toluene, xylenes, and TriMB (trimethylbenzenes) at a response time of ~40 s (Figure 1b), appearing ~4 s later than aliphatic peaks (Figure 1a), ascribed to the stronger adsorption of the former species in the zeolite catalyst. After 40 s, a second broad low-concentration response R2 of benzene (also of toluene and xylenes) is observed around ~60 s, which indicates a secondary formation of aromatics within the H-ZSM-5 catalyst. This broad R2 response of light aromatics disappeared when the catalyst loading was reduced to 4.5 mg (Figure S5), suggesting that the R2 formation of light aromatics is mainly related to secondary reactions occurring in the downstream zone of the catalyst bed in the absence of fully converted MeOH. A detailed discussion on the origin of the second peak of benzene, toluene, and xylenes can be found in our previous paper.[15] It is worth noting that olefins (ethylene, propylene, and butylenes) decay relatively slower than alkanes (methane, ethane, propane, and butanes). The butanes (mainly i-C_4 and some n-C_4) show the highest response, demonstrating their highest product selectivity (Table S2).

To probe the reactivity of HCP species and the proceeding reactions with MeOH, isotopic labeling was used. The experiment was conducted in such way that a series of repetitive ^{13}C-MeOH pulses were sent over a freshly activated H-ZSM-5 catalyst until reaching a quasi-steady-state with unchanging pulse responses. Then a switch was made to ^{12}C-MeOH pulses. An online mass spectrometer monitored the transient evolution of isotopes in the entire experiment. Full testing conditions can be found in the Supporting Information. The results are presented in Figure 2. A sample size of 100 mg H-ZSM-5 zeolite catalyst was selected, ensuring the complete development of hydrocarbon products with decent concentrations for the following statistical isotopic analysis.

The m/z = 91−98 intensities were selected to represent the isotopically labeled and unlabeled toluene, xylenes, and TriMB (all having their most abundant unlabeled fragment at m/z = 91[21]) responses in MTH experiments. During the last ^{13}C-MeOH pulse the most abundant MS fragment, m/z = 98, mainly referring to aromatic fragment $^{13}C_7H_7$, rapidly reaches a maximum and then slowly decays to zero (Figure 2b). MS fragments like m/z = 92 and 91, ascribed to the impurity in ^{13}C-labeling, display a similar trend but of much lower intensity without a tail as m/z = 97 or 98 does, which confirms the full

https://doi.org/10.1021/acscatal.3c00168
ACS Catal. 2023, 13, 5205−5212

labeling of toluene, xylenes, and TriMB before switching to ^{12}C-MeOH.

After switching to ^{12}C-MeOH, in the first pulse response, the fully unlabeled aromatic $^{12}C_7H_7$ fragment, m/z = 91, immediately grows and reaches its maximum with a more than 5-fold higher intensity than those of ^{13}C-containing intermediates (mainly refer to m/z = 92−97, Figure 2a,b). Clearly, the fast formation of aromatics stems mainly from the direct transformation of the newly injected ^{12}C-MeOH. The second most abundant response is a sharp peak at m/z = 98, mainly representing fully labeled species ($^{12}C_7H_7$) directly released upon the first ^{12}C-MeOH pulse even before the appearance of the m/z = 91 peak after switching. This response is attributed to organic species present in the zeolite catalyst sample at the end of the ^{13}C-MeOH pulse series. Comparing the BTX (benzene, toluene, and xylenes) responses from the FASPA experiment (Figure 2a), with the MS responses of m/z = 98 and 91, the latter are perfectly in line with the leading-edge shoulder and the maximum of the temporal BTX responses in the FASPA analysis. This further indicates that the fast appearance of BTX at 35−40 s initially comes from the displacement of retarded species from the previous pulse. A displacement effect by water in the pulse response of toluene/xylene fragments is confirmed by the ^{12}C-MeOH ⇒ H_2O switch experiment presented in Figure 2c, although this is not observed for benzene fragments, probably due to the lower quantity of less retarded benzene (Figure S8). Also, the last product that appeared in the exit flow upon a MeOH pulse is water (m/z = 18, Figure S6), confirming that the adsorption of water in the catalyst bed is stronger than that of aromatics and aliphatics under operating conditions.[22−24] After the displacement process, the MS peak of m/z = 91 has a much higher intensity than those of m/z = 92−97, suggesting that newly formed aromatics predominantly stem from the newly injected ^{12}C-MeOH.

Similar results were obtained when the pulsing interval was reduced from 3.75 to 1.25 min, resulting in an even larger displacement response at m/z = 98 upon the first ^{12}C-MeOH pulse (Figure S9c). The decreasing intensity of benzene and toluene signal over the pulse time (20−26 s in Figure S9b) before their breakthrough supports the interpretation of an unfinished decomposition/desorption process for these species out of the catalyst bed from the previous pulse. It is also evidenced by the slightly lower carbon selectivity and the 0th moment μ_0 of aromatics (TriMB and BTX, Table S2) when reducing the pulsing interval from 3.75 to 1.25 min.

The isotopic ^{13}C−^{12}C distribution in selected products during the switch was followed by monitoring the MS signals in the range of m/z = 91−98, representative for C_7H_7 fragment contributions of TriMB, xylenes, and toluene, in the range m/z = 39−47 representative for C_{3+} aliphatics fragments. The isotopic distribution of the C_7 aromatics upon the first ^{12}C-MeOH pulse based on the m/z = 91−98 MS responses corrected for fragmentation and the overall ^{13}C−^{12}C atomic content in each pulse are presented in Figure 3, including the theoretical case for a random isotope distribution in MS fragment C_7H_7 based on the same ^{13}C−^{12}C atomic content.[1] The full random distribution pattern as function of ^{13}C−^{12}C content is given by Figure S7 in Supporting Information. There is no difference in the reactivity of these different isotopic fragments in the MTH reactions.[1]

The estimated ^{13}C−^{12}C distribution in Figure 3 suggests that 15 at % of the total C first leaves the catalyst bed in the

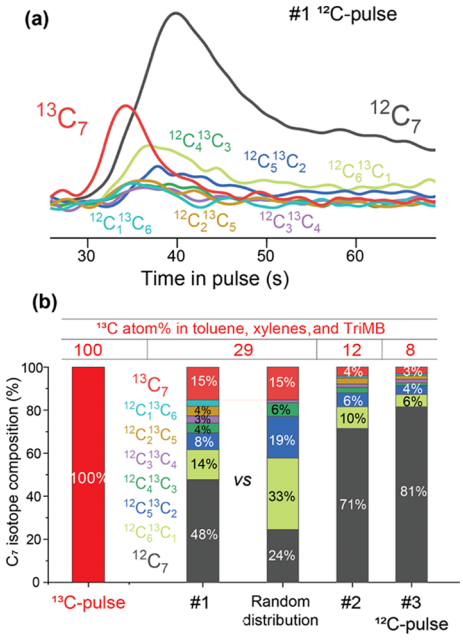

Figure 3. Contributions of C_7 aromatics (formula $^{12}C_n{}^{13}C_{7-n}$, n = 0−7) from MS responses at m/z = 91−98 corrected for fragmentation upon the first ^{12}C-MeOH pulse after repetitive pulsing ^{13}C-MeOH (top) and corresponding C_7 isotope composition (bottom) with the ^{13}C content (at %) in the last ^{13}C-MeOH pulse response and the following three ^{12}C-MeOH pulse responses, pulse interval = 3.75 min. The ^{13}C content in the displacement peak, m/z = 98 is not taken into account to estimate the random distribution of ^{13}C in m/z = 91−98 aromatic fragments.

form of the fully labeled $^{13}C_7$ (originating from toluene, xylenes or TriMB) during the abovementioned displacement process. On the other hand, 48 at % C-content was observed in the form of fully unlabeled $^{12}C_7$ (mainly from m/z = 91), directly after the displacement process, which completely stems from the newly injected ^{12}C-MeOH. The isotopic mixed products are based on the fragment intermediates from m/z = 92 to 97. In total, 29 at % ^{13}C was collected during the first ^{12}C-MeOH pulse response arising from the displacement (15 at %) and the following mixed isotope products (14 at %). In the second and third ^{12}C-MeOH pulse responses the ^{13}C content quickly dropped, indicating that the ^{13}C-HCP is replaced by a few repeated ^{12}C-MeOH pulses.

In a random distribution model with the same ^{13}C/^{12}C atomic ratio (14/71 at % ignoring the displacement process), the most abundant isotopic aromatic species would be $^{13}C_1{}^{12}C_6$, followed by $^{13}C_2{}^{12}C_5$, $^{13}C_3{}^{12}C_4$, and $^{12}C_7$. This differs completely from the observed ^{13}C−^{12}C distribution, in which $^{12}C_7$ shows a higher contribution in the first ^{12}C-MeOH pulse response. Note that 15 at % ^{13}C in the form of $^{13}C_7$ directly leaves the bed without participating in the consecutive reactions and is accordingly not taken into account in this model.

When shortening the MeOH pulsing interval to 1.25 min (faster pulsing), the total ^{13}C content in aromatic C_7 isotopic compounds in the first ^{12}C-MeOH pulse response after switching is 46 at % (Figure S9d), higher than the 29 at % for 3.75 min pulse interval, indicating more retarded organic species are present in the catalyst. Still, in comparison with a random distribution, a much higher contribution of $^{12}C_7$ (from

https://doi.org/10.1021/acscatal.3c00168
ACS Catal. 2023, 13, 5205−5212

fully unlabeled toluene, xylenes, or TriMB) is observed in the first ^{12}C-MeOH pulse response.

The MS responses for the C_6 benzene isotopes (Figure 4, left) show the same two important trends as for the C_7 aromatic isotopes: A clear displacement response of the full ^{13}C-benzene isotope for the 1.25 min pulse interval, which is hardly observed after the longer pulse interval of 3.75 min due to prolonged wash-out; An appearance of mixed isotopes with maxima in sequential temporal order from pure $^{13}C_6$, followed by $^{13}C_5{}^{12}C$, $^{13}C_4{}^{12}C_2$, $^{13}C_3{}^{12}C_3$, $^{13}C_2{}^{12}C_4$, and $^{13}C^{12}C_5$ to finally pure $^{12}C_6$.

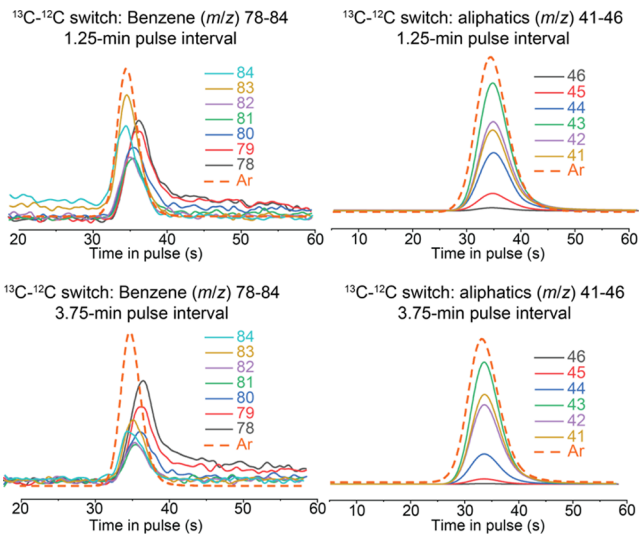

Figure 4. MS responses of benzene fragments (m/z = 78−84, left) and aliphatic fragments (m/z = 41−46, right) in the first ^{12}C-MeOH pulse in MeOH switch experiments at 400 °C over 100 mg catalyst. Pulse size used 7.6 μmol_C/pulse.

The incorporation of the carbon isotope in the light aliphatic products was also analyzed from the C_3 MS response signals at m/z = 39−47, comprising mainly contributions from the major products propylene, *iso*- and *n*-butane, and propane. Due to the argon tracer co-injection, m/z = 40 was not used. The fragmentation patterns of the quasi-steady-state responses of ^{13}C-MeOH pulses and ^{12}C-MeOH pulses served as references (Table S3). It is assumed that upon the $^{13}C/^{12}$C-MeOH switch, the component (molar) response composition does not change, but only the isotopic composition, and that these components behave similarly with regards to fragmentation in the mass spectrometer. Then, the pure component fragmentation patterns for each species are not needed for the isotopic mixture analysis; only the data of the pure ^{12}C or ^{13}C product pulses after shifting 1, 2, or 3 m/z units for the different C_3 fragments ($^{12}C_3$, $^{12}C_2{}^{13}C$, $^{12}C^{13}C_2$, and $^{13}C_3$). The isotopic composition analysis of the first ^{12}C-MeOH pulse after switching from ^{13}C-MeOH was performed by the constrained parameter estimation of the linear combinations in Athena Visual Studio[25] with zero value as the lower limit (see Section S2 in Supporting Information for further details).

As concluded from Figure 4, the light aliphatics do not exhibit the displacement response observed for aromatics. In addition, no indication for fully labeled $^{13}C_3$ species was obtained for the fragmentation patterns in the 3.75 min case and only a tiny percentage (3%) for the 1.25 min case (Table S1, Figure 5). The total ^{13}C contents in isotopic C_3 components are approximately 7 and 33 at % for the 3.75 and 1.25 min pulse intervals, respectively, indicating much less ^{13}C-HCP species with increasing pulsing interval. The random distribution model in both cases (3.75 and 1.25 min pulse intervals) predicts a similar isotopic composition, as observed (Figure 5c), suggesting a fast isotope scrambling process in the investigated C_{3+} species.

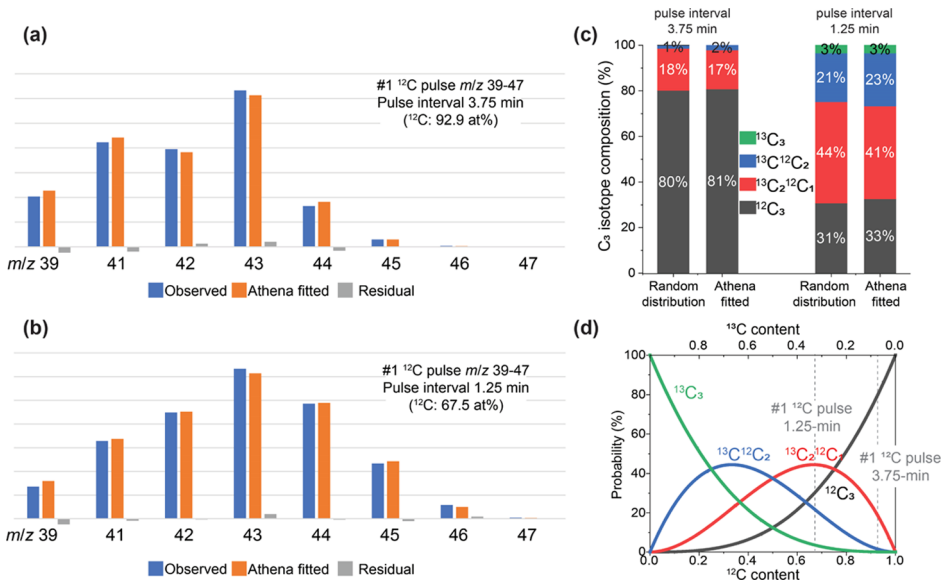

Figure 5. MS analysis of m/z = 39−47 for C_{3+} components produced upon the first ^{12}C-MeOH pulse after switching. The fitted MS fragmentation pattern for 3.75 min (a) and 1.25 min (b) pulse interval; (c) comparison of fitted MS isotope composition with that of a random distribution assuming the same $^{13}C/^{12}$C content as in (a,b); (d) random distribution isotope composition for m/z = 39−47 as a function of $^{13}C/^{12}$C content. Dashed lines refer to the estimated $^{13}C-^{12}$C contents in the first ^{12}C-MeOH pulse for 1.25 and 3.75 min pulse interval, respectively.

https://doi.org/10.1021/acscatal.3c00168
ACS Catal. 2023, 13, 5205−5212

DISCUSSION

Combining the product responses from the FASPA tests and the online MS analysis yields unprecedented gas phase product information for unraveling consecutive reaction steps such as aromatic displacement, HCP reactions and secondary reactions following a MeOH pulse. The subsequent statistical analysis of characteristic MS fragmentation/isotope compositions in the $^{13}C-^{12}C$ switch experiments reveals a faster isotope scrambling process in olefin products than that in aromatics, providing direct experimental confirmation of the kinetically preferred olefin-based rather than the aromatic-based reaction mechanism. Analysis of the full range of MS signals m/z = 91−98 referring to ^{13}C-aromatics with a formula of $^{12}C_n{}^{13}C_{7-n}$ (n = 0−7) yielded a different composition than according to the random distribution, suggesting a rate-limited incorporation process of all carbons from newly injected MeOH into aromatic HCP species.

For the used medium pore size H-ZSM-5 zeolite catalyst, a dual-cycle (olefin and aromatic cycle) mechanism involving the consecutive methylation/cracking of olefins and alkylation/split-off of aromatics, respectively, has been accepted to account for the production of olefins and light aromatics.[16] The aromatic cycle is further categorized into paring and side-chain mechanistic routes initially for a CHA-type zeolite catalyst, like H-SAPO-34. In the paring mechanism,[26,27] the contraction of an aromatic ring generates methylated cyclopentadienyl/cyclopentenyl species[2,6] (or methylenecyclopentenyl species[13]), which then undergo cracking reactions to split off light olefins. The final step is the methylation of five-membered ring cations followed by ring expansion (isomerization) eventually closing the cycle (Figure 6). In the side-chain mechanism,[28] the deprotonation of heptamethylbenzenium ions generates a C=C double bond in the alkyl side groups on the benzene ring. The further methylation followed by dealkylation of the alkyl side group produces ethylene, whereas a multimethylation/dealkylation produces longer olefins. An important distinction between these two mechanisms is that in the paring route, carbon atoms from the benzene ring end up in products and not in the side-chain route. The former predicts mixed isotopic aromatic species in the isotopic switch experiments of MeOH pulses.

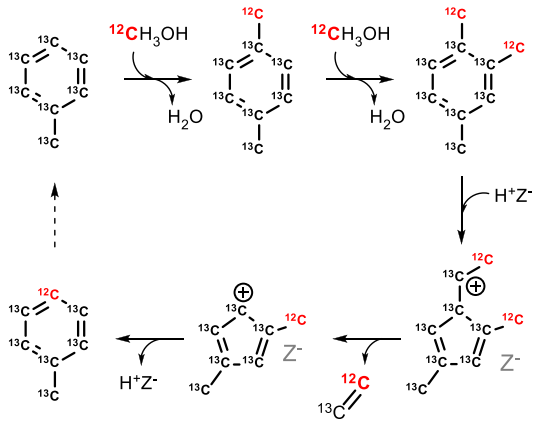

Figure 6. Scheme of $^{13}C/^{12}C$ isotopic incorporating process in the paring mechanism via cyclopentadienyl cations[2,6] in the MTH process when a ^{13}C-MeOH pulse is switched to a ^{12}C-MeOH pulse. Note: an alternative paring mechanism via the methylenecyclopentenyl cations was recently proposed by Studt et al.[13]

Leaving the displacement phenomenon of aromatics out of consideration, a random distribution of ^{12}C in ^{13}C-aromatics, which relies on the assumption of the equal reactivity of ^{13}C atoms in the ^{13}C-containing HCP species (still present after the last ^{13}C-MeOH pulse), toward the newly fed ^{12}C reactant, is not observed (Figure 3). Instead, the observed C_7 isotope compositions suggest a finite incorporation rate of ^{12}C into ^{13}C-containing aromatics next to a rapid build-up of new aromatics. This latter production of aromatics mainly stems from the direct aromatization of newly injected ^{12}C-MeOH, leading to the dominant contribution of $^{12}C_7$ (m/z = 91) already in the first ^{12}C-MeOH pulse response, much higher than a random distribution predicts (Figure 3). A sequential temporal appearance of $^{12}C_1{}^{13}C_6$ to $^{12}C_6{}^{13}C_1$ (mainly referring to m/z = 97 to 92, Figure 3a, S9c) and m/z = 84 to 78 (referring to the fully labeled to fully unlabeled C_6 components, Figure 4 left) indeed shows a successive incorporation of ^{12}C into the present ^{13}C aromatics, ultimately replacing all ^{13}C atoms. This finding suggests an operational role for the paring route (Figure 6) in the aromatic cycle.

To compare, the analysis of the $^{12}C-^{13}C$ composition for C_{3+} aliphatics gave a pattern highly similar to that predicted by the random distribution model (Figure 5c), indicating a fast incorporation of ^{12}C into ^{13}C-containing aliphatics, which is consistent with the higher activity of the olefin cycle than the aromatic cycle[29,30] for the production of light aliphatics in the H-ZSM-5 zeolite catalyst.

For the displacement peak of light aromatics upon the first ^{12}C-MeOH/water pulse (Figures 2 and 3), we speculate that these retarded organic species are displaced mainly by water, stemming from the fast dehydration of MeOH. The DFT-calculated adsorption energy of MeOH, water, and related hydrocarbons decreases in the order MeOH (−105 kJ/mol[31]) > water (−83 kJ/mol[31]) > toluene/p-xylenes (−62/−71 kJ/mol[15,32]) > ethylene/propylene (−37/−53 kJ/mol[33]). Further evidence arises from the delayed appearance of water in the exit flow after olefins and aromatics upon a MeOH pulse (Figure S6). Clearly, water competes with olefins and aromatics occupying part of Brønsted acid sites, which makes them only accessible for MeOH and pushes out primarily formed aromatics.[34−36] This also explains why cofeeding water in the MTH process allows increasing the selectivity to olefins and prolonging the catalyst's lifetime.[36,37]

Finally, based on the FASPA analysis and $^{13}C/^{12}C$ switch experiments, the processes leading to aromatic products upon MeOH pulsing to a working H-ZSM-5 zeolite catalyst in the MTH process are schematically summarized in Figure 7. Upon MeOH arriving at the active zone of the catalyst bed, all products are immediately formed after a rather short induction period. Water first displaces retarded aromatic HCP species still retained in the catalyst bed from the previous MeOH pulse, resulting in the first fast appearance of aromatics in the exit flow (contribution no. 1). In the presence of MeOH, the remaining labeled HCP species further react with unlabeled MeOH, predominantly forming aliphatics via the cracking reactions and aromatics via the paring route (contribution no. 2). Meanwhile, the olefinic cycle and direct aromatization of MeOH are also operative, giving the major production of new unlabeled aromatics represented by contribution no. 3. In the end, the broad aromatic contribution no. 4 in Figure 7 comprises the secondary formation of aromatics from the decomposition/desorption of primarily formed HCP species and retarded olefins in the absence of MeOH, which has been

https://doi.org/10.1021/acscatal.3c00168
ACS Catal. 2023, 13, 5205−5212

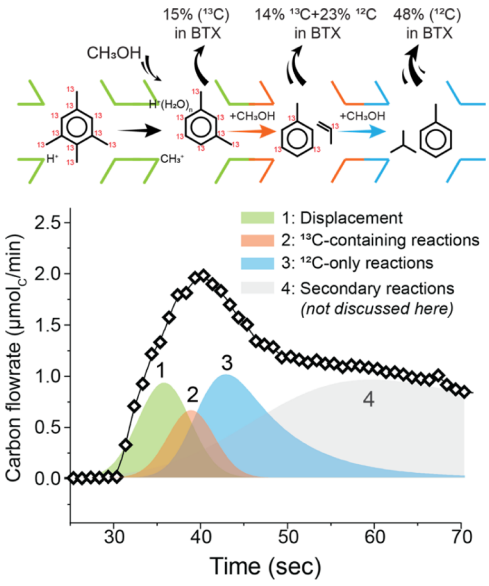

Figure 7. Schematic illustration of aromatic products formation processes in MTH upon ^{12}C-MeOH pulse into H-ZSM-5 with prebuilt ^{13}C-HCP. Reaction conditions are given in Figure 1.

discussed in our previous work.[15] This fourth contribution is only observed for catalyst beds after full MeOH conversion. The relative contributions of these four processes depend on the pulse size and injection frequency relative to the catalyst amount. Under continuous MTH operation, these processes will occur simultaneously, and the product composition will be a convolution of their contributions.

CONCLUSIONS

The MTH process over zeolites offers a sustainable route to produce important commodities, such as light olefins and aromatics. Depending on the pore structure of utilized zeolites, the dominant MTH reaction path in the HCP mechanism varies and exhibits different properties. By applying newly developed FASPA and isotopic labeling, the highly interweaved reactions upon a MeOH pulse to a model H-ZSM-5 zeolite catalyst were decoupled into several consecutive steps, including the fast aromatic displacement by water, rapid reactions between MeOH and retained hydrocarbons (HCP), including a fast direct MeOH aromatization, and secondary reactions in the catalyst in the absence of MeOH. The isotope analysis of the pulse response products in the ^{13}C-MeOH/^{12}C-MeOH switch experiments provides direct experimental confirmation for the kinetically favored reactions of the olefin cycle over the aromatic cycle in the dual-cycle mechanism.

The observation of the complete sequential incorporation of ^{12}C atoms into ^{13}C-aromatics in the isotope switch experiments suggests an operational role of the paring route in the aromatic cycle.

ASSOCIATED CONTENT

Supporting Information

The Supporting Information is available free of charge at https://pubs.acs.org/doi/10.1021/acscatal.3c00168.

Chemicals and zeolite materials, structural characterization, and experimental and analytical methods and results (PDF)

AUTHOR INFORMATION

Corresponding Authors

Evgeny A. Pidko − *Inorganic Systems Engineering, Department of Chemical Engineering, Delft University of Technology, 2629 HZ Delft, The Netherlands;* orcid.org/0000-0001-9242-9901; Email: e.a.pidko@tudelft.nl

Freek Kapteijn − *Catalysis Engineering, Department of Chemical Engineering, Delft University of Technology, 2629 HZ Delft, The Netherlands;* orcid.org/0000-0003-0575-7953; Email: F.Kapteijn@tudelft.nl

Authors

Chuncheng Liu − *Inorganic Systems Engineering, Department of Chemical Engineering, Delft University of Technology, 2629 HZ Delft, The Netherlands; Catalysis Engineering, Department of Chemical Engineering, Delft University of Technology, 2629 HZ Delft, The Netherlands*

Evgeny A. Uslamin − *Inorganic Systems Engineering, Department of Chemical Engineering, Delft University of Technology, 2629 HZ Delft, The Netherlands;* orcid.org/0000-0001-5454-9582

Complete contact information is available at: https://pubs.acs.org/10.1021/acscatal.3c00168

Author Contributions

The manuscript was written through the contributions of all authors. All authors have given their approval to the final version of the manuscript.

Notes

The authors declare no competing financial interest.

ACKNOWLEDGMENTS

We acknowledge BASF and the Advanced Research Center Chemical Building Blocks Consortium (ARC CBBC) for funding under project number 2016.007.TUD.

REFERENCES

(1) Dahl, I. M.; Kolboe, S. On the reaction mechanism for propene formation in the MTO reaction over SAPO-34. *Catal. Lett.* **1993**, *20*, 329−336.

(2) Olsbye, U.; Svelle, S.; Bjørgen, M.; Beato, P.; Janssens, T. V. W.; Joensen, F.; Bordiga, S.; Lillerud, K. P. Conversion of Methanol to Hydrocarbons: How Zeolite Cavity and Pore Size Controls Product Selectivity. *Angew. Chem., Int. Ed.* **2012**, *51*, 5810−5831.

(3) Ilias, S.; Bhan, A. Mechanism of the Catalytic Conversion of Methanol to Hydrocarbons. *ACS Catal.* **2013**, *3*, 18−31.

(4) Bjørgen, M.; Svelle, S.; Joensen, F.; Nerlov, J.; Kolboe, S.; Bonino, F.; Palumbo, L.; Bordiga, S.; Olsbye, U. Conversion of methanol to hydrocarbons over zeolite H-ZSM-5: On the origin of the olefinic species. *J. Catal.* **2007**, *249*, 195−207.

(5) Yarulina, I.; Chowdhury, A. D.; Meirer, F.; Weckhuysen, B. M.; Gascon, J. Recent trends and fundamental insights in the methanol-to-hydrocarbons process. *Nat. Catal.* **2018**, *1*, 398−411.

(6) Van Speybroeck, V.; Hemelsoet, K.; Joos, L.; Waroquier, M.; Bell, R. G.; Catlow, C. R. A. Advances in theory and their application within the field of zeolite chemistry. *Chem. Soc. Rev.* **2015**, *44*, 7044−7111.

(7) Wang, C.; Chu, Y.; Zheng, A.; Xu, J.; Wang, Q.; Gao, P.; Qi, G.; Gong, Y.; Deng, F. Frontispiece: New Insight into the Hydrocarbon-Pool Chemistry of the Methanol-to-Olefins Conversion over Zeolite H-ZSM-5 from GC-MS, Solid-State NMR Spectroscopy, and DFT Calculations. *Chem.—Eur. J.* **2014**, *20*, 12432−12443.

(8) Vedrine, J. C.; Dejaifve, P.; Garbowski, E. D.; Derouane, E. G. Aromatics Formation from Methanol and Light Olefins Conversions

on H-ZSM-5 Zeolite: Mechanism and Intermediate Species. *Stud. Surf. Sci. Catal.* **1980**, *5*, 29−37.
(9) Goguen, P. W.; Xu, T.; Barich, D. H.; Skloss, T. W.; Song, W.; Wang, Z.; Nicholas, J. B.; Haw, J. F. Pulse-Quench Catalytic Reactor Studies Reveal a Carbon-Pool Mechanism in Methanol-to-Gasoline Chemistry on Zeolite HZSM-5. *J. Am. Chem. Soc.* **1998**, *120*, 2650−2651.
(10) Xu, S.; Zheng, A.; Wei, Y.; Chen, J.; Li, J.; Chu, Y.; Zhang, M.; Wang, Q.; Zhou, Y.; Wang, J.; Deng, F.; Liu, Z. Direct Observation of Cyclic Carbenium Ions and Their Role in the Catalytic Cycle of the Methanol-to-Olefin Reaction over Chabazite Zeolites. *Angew. Chem., Int. Ed. Engl.* **2013**, *52*, 11564−11568.
(11) Wulfers, M. J.; Jentoft, F. C. The Role of Cyclopentadienium Ions in Methanol-to-Hydrocarbons Chemistry. *ACS Catal.* **2014**, *4*, 3521−3532.
(12) Hernandez, E. D.; Jentoft, F. C. Spectroscopic Signatures Reveal Cyclopentenyl Cation Contributions in Methanol-to-Olefins Catalysis. *ACS Catal.* **2020**, *10*, 5764−5782.
(13) Plessow, P. N.; Enss, A. E.; Huber, P.; Studt, F. A new mechanistic proposal for the aromatic cycle of the MTO process based on a computational investigation for H-SSZ-13. *Catal. Sci. Technol.* **2022**, *12*, 3516−3523.
(14) Sun, X.; Mueller, S.; Liu, Y.; Shi, H.; Haller, G. L.; Sanchez-Sanchez, M.; van Veen, A. C.; Lercher, J. A. On reaction pathways in the conversion of methanol to hydrocarbons on HZSM-5. *J. Catal.* **2014**, *317*, 185−197.
(15) Liu, C.; Uslamin, E. A.; Pidko, E. A.; Kapteijn, F. Direct discerning reaction pathways in methanol-to-hydrocarbons by transient operation − FASPA. *J. Chem. Eng.* **2023**, *453*, 139696.
(16) Svelle, S.; Joensen, F.; Nerlov, J.; Olsbye, U.; Lillerud, K.-P.; Kolboe, S.; Bjørgen, M. Conversion of methanol into hydrocarbons over zeolite H-ZSM-5: Ethene formation is mechanistically separated from the formation of higher alkenes. *J. Am. Chem. Soc.* **2006**, *128*, 14770−14771.
(17) Redekop, E. A.; Lazzarini, A.; Bordiga, S.; Olsbye, U. A Temporal Analysis of Products (TAP) Study of C_2-C_4 Alkene Reactions with a well-defined pool of methylating species on ZSM-22 zeolite. *J. Catal.* **2020**, *385*, 300−312.
(18) Brogaard, R. Y.; Henry, R.; Schuurman, Y.; Medford, A. J.; Moses, P. G.; Beato, P.; Svelle, S.; Nørskov, J. K.; Olsbye, U. Methanol-to-hydrocarbons conversion: The alkene methylation pathway. *J. Catal.* **2014**, *314*, 159−169.
(19) Dessau, R. M.; LaPierre, R. B. On the mechanism of methanol conversion to hydrocarbons over HZSM-5. *J. Catal.* **1982**, *78*, 136−141.
(20) Cesarini, A.; Mitchell, S.; Zichittella, G.; Agrachev, M.; Schmid, S. P.; Jeschke, G.; Pan, Z.; Bodi, A.; Hemberger, P.; Pérez-Ramírez, J. Elucidation of radical- and oxygenate-driven paths in zeolite-catalysed conversion of methanol and methyl chloride to hydrocarbons. *Nat. Catal.* **2022**, *5*, 605−614.
(21) NIST/EPA/NIH Mass Spectral Library (EI); National Institute of Standards and Technology. https://www.nist.gov/srd/nist-standard-referencedatabase-1a/(accessed Sept, 2022).
(22) Ison, A.; Gorte, R. J. The adsorption of methanol and water on H-ZSM-5*1. *J. Catal.* **1984**, *89*, 150−158.
(23) Wang, S.; Chen, Y.; Wei, Z.; Qin, Z.; Ma, H.; Dong, M.; Li, J.; Fan, W.; Wang, J. Polymethylbenzene or Alkene Cycle? Theoretical Study on Their Contribution to the Process of Methanol to Olefins over H-ZSM-5 Zeolite. *J. Phys. Chem. C* **2015**, *119*, 28482−28498.
(24) Fečík, M.; Plessow, P. N.; Studt, F. A Systematic Study of Methylation from Benzene to Hexamethylbenzene in H-SSZ-13 Using Density Functional Theory and Ab Initio Calculations. *ACS Catal.* **2020**, *10*, 8916−8925.
(25) *AthenaVisual Studio*; Athenavisual, Inc., 2022. https://athenavisual.com/ (accessed Oct, 2022).
(26) Sullivan, R. F.; Egan, C. J.; Langlois, G. E.; Sieg, R. P. A New Reaction That Occurs in the Hydrocracking of Certain Aromatic Hydrocarbons. *J. Am. Chem. Soc.* **1961**, *83*, 1156−1160.
(27) Lesthaeghe, D.; Horré, A.; Waroquier, M.; Marin, G. B.; Van Speybroeck, V. Theoretical Insights on Methylbenzene Side-Chain Growth in ZSM-5 Zeolites for Methanol-to-Olefin Conversion. *Chem.—Eur. J.* **2009**, *15*, 10803−10808.
(28) Mole, T.; Bett, G.; Seddon, D. Conversion of methanol to hydrocarbons over ZSM-5 zeolite: An examination of the role of aromatic hydrocarbons using ^{13}carbon- and deuterium-labeled feeds. *J. Catal.* **1983**, *84*, 435−445.
(29) Kumar, P.; Thybaut, J. W.; Svelle, S.; Olsbye, U.; Marin, G. B. Single-Event Microkinetics for Methanol to Olefins on H-ZSM-5. *Ind. Eng. Chem. Res.* **2013**, *52*, 1491−1507.
(30) Standl, S.; Hinrichsen, O. Kinetic Modeling of Catalytic Olefin Cracking and Methanol-to-Olefins (MTO) over Zeolites: A Review. *Catalysts* **2018**, *8*, 626.
(31) Van der Mynsbrugge, J.; Moors, S. L. C.; De Wispelaere, K.; Van Speybroeck, V. Insight into the Formation and Reactivity of Framework-Bound Methoxide Species in H-ZSM-5 from Static and Dynamic Molecular Simulations. *ChemCatChem* **2014**, *6*, 1906−1918.
(32) Jentys, A.; Mukti, R. R.; Tanaka, H.; Lercher, J. A. Energetic and entropic contributions controlling the sorption of benzene in zeolites. *Microporous Mesoporous Mater.* **2006**, *90*, 284−292.
(33) Svelle, S.; Tuma, C.; Rozanska, X.; Kerber, T.; Sauer, J. Quantum Chemical Modeling of Zeolite-Catalyzed Methylation Reactions: Toward Chemical Accuracy for Barriers. *J. Am. Chem. Soc.* **2009**, *131*, 816−825.
(34) Marchi, A. J.; Froment, G. F. Catalytic conversion of methanol to light alkenes on SAPO molecular sieves. *Appl. Catal.* **1991**, *71*, 139−152.
(35) Wu, X.; Anthony, R. G. Effect of feed composition on methanol conversion to light olefins over SAPO-34. *Appl. Catal., A* **2001**, *218*, 241−250.
(36) De Wispelaere, K.; Wondergem, C. S.; Ensing, B.; Hemelsoet, K.; Meijer, E. J.; Weckhuysen, B. M.; Van Speybroeck, V.; Ruiz-Martínez, J. Insight into the Effect of Water on the Methanol-to-Olefins Conversion in H-SAPO-34 from Molecular Simulations and in Situ Microspectroscopy. *ACS Catal.* **2016**, *6*, 1991−2002.
(37) Wang, H.; Hou, Y.; Sun, W.; Hu, Q.; Xiong, H.; Wang, T.; Yan, B.; Qian, W. Insight into the Effects of Water on the Ethene to Aromatics Reaction with HZSM-5. *ACS Catal.* **2020**, *10*, 5288−5298.

https://doi.org/10.1021/acscatal.3c00168
ACS Catal. 2023, 13, 5205−5212